ADVANCED FUNCTIONAL MATERIALS
www.afm-journal.de

Graphene Potentiates the Myocardial Repair Efficacy of Mesenchymal Stem Cells by Stimulating the Expression of Angiogenic Growth Factors and Gap Junction Protein

Jooyeon Park, Yong Sook Kim, Seungmi Ryu, Wan Seok Kang, Subeom Park, Jin Han, Hae Chang Jeong, Byung Hee Hong, Youngkeun Ahn, and Byung-Soo Kim**

Stem cell therapy has emerged as a potential modality for myocardial infarction treatment. Mesenchymal stem cells (MSCs) exert reparative actions in the injured myocardium mainly through the secretion of paracrine factors. In addition, the overexpression of connexin 43 (Cx43), a gap junction protein, promotes cardiac repair and function restoration. It is known that MSCs in a spheroid form, which have enhanced cell–cell interaction, exhibit enhanced expression of paracrine factors and Cx43. However, cell-extracellular matrix (ECM) interactions, which also contribute to growth factor expression, are very limited in MSC spheroids. Reduced graphene oxide (RGO) shows high affinity toward ECM proteins, such as fibronectin (FN), and high electrical conductivity. In this study, by incorporating FN-adsorbed RGO flakes into MSC spheroids, it is possible to enhance the cell–ECM interactions and, subsequently, the paracrine factor expression in the MSCs in spheroids. Cx43 is also upregulated likely due to the enhanced paracrine factor expression and electrical conductivity of RGO. The injection of MSC–RGO hybrid spheroids into the infarcted hearts enhances cardiac repair compared with the injection of RGO flakes or MSC spheroids. This study demonstrates that RGO can effectively improve the therapeutic efficacy of MSCs for ischemic heart diseases.

J. Park, J. Han, Prof. B.-S. Kim
School of Chemical and Biological Engineering
Seoul National University
Seoul 151-744, Republic of Korea
E-mail: byungskim@snu.ac.kr
Y. S. Kim, W. S. Kang, H. C. Jeong, Prof. Y. Ahn
Department of Cardiology
Chonnam National University Hospital
Gwangju 501-757, Republic of Korea
E-mail: cecilyk@jnu.ac.kr
S. Ryu, Prof. B.-S. Kim
Interdisciplinary Program of Bioengineering
Seoul National University
Seoul 151-744, Republic of Korea
S. Park, Prof. B. H. Hong
Department of Chemistry
Seoul National University
Seoul 151-747, Republic of Korea
Prof. B.-S. Kim
Bio-MAX Institute, Institute of Chemical Processes
Engineering Research Institute
Seoul National University
Seoul 151-744, Korea

DOI: 10.1002/adfm.201500365

1. Introduction

Mesenchymal stem cell (MSC) implantation is a promising strategy for cardiac repair after myocardial infarction (MI).[1] Previous studies have demonstrated that MSCs implanted into the ischemic myocardium contribute to the induction of angiogenesis, attenuation of cardiac remodeling, and improvement in cardiac functions mainly through the secretion of reparative paracrine factors.[2] Meanwhile, MI may enhance vulnerability to arrhythmia due to gap junction remodeling as a result of cardiac fibrosis and the loss of gap junction-expressing cardiac cells.[3] The implantation of cells expressing gap junction proteins, such as connexin 43 (Cx43), can attenuate postinfarct arrhythmia.[4] Although MSCs are capable of expressing Cx43, the amount of Cx43 expressed by naïve MSCs is minimal,[5] raising concerns regarding their proarrhythmogenic potential.[6] In addition, the upregulated expression of Cx43 in MSCs enhances their cytoprotective effect on cardiomyocytes and improves cardiac function.[7] Therefore, the upregulation of reparative paracrine factors and Cx43 expression in MSCs would enhance the therapeutic efficacy and reduce the risk of arrhythmia in MSC implantation therapy for MI.

The implantation of MSCs into the infarcted myocardium in a spheroid form may be advantageous because MSCs in spheroids show enhanced expression of angiogenic growth factors, such as vascular endothelial growth factor (VEGF) and fibroblast growth factor-2 (FGF-2),[8] and Cx43.[9] The enhanced cell–cell interactions in MSC spheroids promote the expression of reparative paracrine factors.[10] Additionally, this, at least in part, contributes to the upregulation of Cx43 expression.[11] However, cells in spheroid form show poor cell–extracellular matrix (ECM) interactions,[12] which may limit further stimulation of growth factor expression and thereby Cx43 expression.[13]

In this study, we hypothesized that the incorporation of reduced graphene oxide (RGO) flakes into MSC spheroids would improve the expression of reparative paracrine factors and Cx43 in the MSCs. RGO is a 2D nanomaterial composed of carbon atoms, showing unique optical, chemical, mechanical,

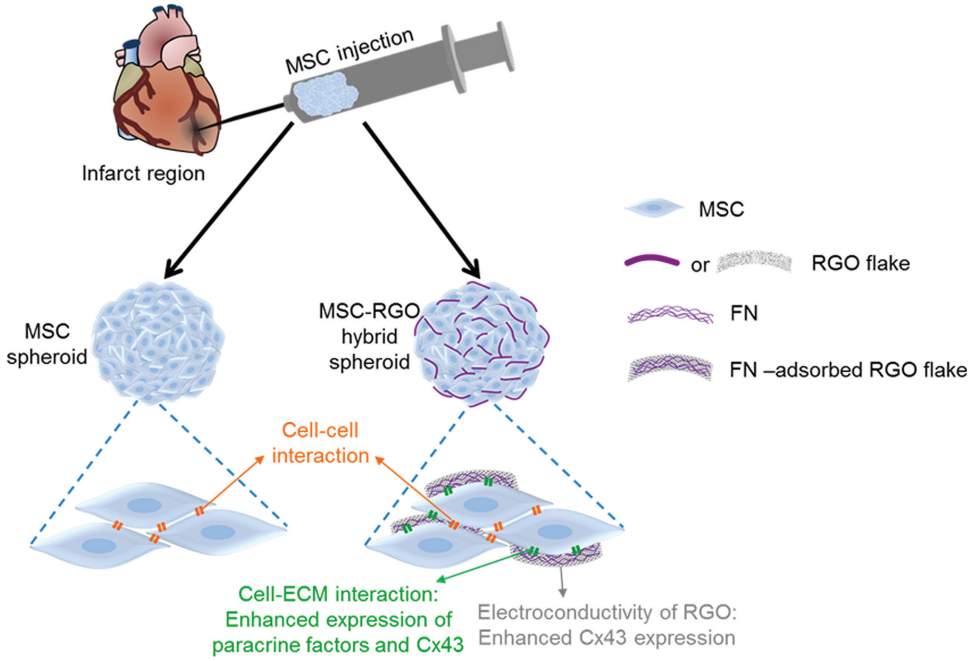

Figure 1. Schematic illustration of the effects of RGO flake incorporation in MSC spheroids on cardiac repair in MSC therapy for the treatment of MI.

and electrical properties.[14] Cellular interactions with electrically conductive materials enhance Cx43 expression.[15] In addition, RGO is capable of adsorbing ECM proteins, such as fibronectin (FN), from the serum contained in the cell culture medium.[16] This feature of RGO can provide cell–ECM interactions,[17] which can enhance the expression of paracrine factors[18] and Cx43.[19] Therefore, we investigated whether the incorporation of RGO flakes into MSC spheroids can enhance the expression of reparative paracrine factors and Cx43 in the MSCs and the therapeutic efficacy of the MSCs for the treatment of MI (**Figure 1**).

2. Results and Discussion

2.1. Characterization of RGO Flakes

The Raman spectrum of RGO flakes showed two characteristic peaks of graphene at 1580 and 1350 cm^{-1}, which are known as G and D band, respectively (**Figure 2**a).[20] The atomic force microscopy (AFM) image of RGO flakes showed that the thickness of the RGO flakes used in this study was ≈1–2 nm (Figure 2b). The AFM and transmission electron microscopy (TEM) images showed that the sizes of the RGO flakes were ≈2–5 μm (Figure 2b,c). RGO flakes with such sizes were used to enhance the cell–ECM interactions and cell–cell interactions. RGO flakes larger than 2 μm were used because RGO flakes under 1 μm can be easily internalized by the cells.[21] The adhesion of RGO flakes to MSCs, rather than internalization of RGO flakes into MSCs, is needed to promote cell–ECM interactions. RGO flakes smaller than 5 μm were used to prevent RGO flakes from physically hindering cell–cell interactions between MSCs with the size ranging from 15 to 19 μm.[22] The sixfold symmetry of the selected area electron diffraction (SAED) pattern image (inset) obtained through TEM showed the high crystallinity of the RGO used in our experiments (Figure 2c). The intensity profile of the diffraction peaks measured along the denoted line showed that the intensities of the $\bar{1}0\bar{1}0$ (inner hexagon) and $\bar{1}\bar{1}20$ (outer hexagon) spots were similar, which demonstrates that the RGO flakes used in this study were close to single layer (Figure 2c).[23]

2.2. Formation of MSC–RGO Hybrid Spheroids

Previous studies have demonstrated that the use of various materials can influence the functions of cells in spheroids. For example, embryonic bodies cultured on hydrogel materials with controlled elasticity showed enhanced formation of cardiovascular organoids.[14] Recently, Yoon et al. have reported that the incorporation of transforming growth factor-β3-adsorbed graphene oxide (GO) sheets to spheroids improved the chondrogenic differentiation of the adipose-derived stem cells.[12] In this study, we utilized the potential of RGO flakes to enhance cell–ECM interactions and the electrical conductivity of RGO flakes to enhance the function of MSCs.

To determine the optimal concentration of RGO flakes for the formation of MSC–RGO hybrid spheroids, the cytotoxicity of the RGO flakes at various concentrations was examined. The 4′,6-diamidino-2-phenylindole (DAPI) staining of cell nucleus and terminal deoxynucleotidyl transferase dUTP nick end labeling (TUNEL) staining of apoptotic cells demonstrated that the incorporation of RGO flakes into MSC spheroids by adding RGO flakes at concentrations of 0, 2.5, 5, and 10 μg mL^{-1} to MSC suspensions in hanging drop form (Sph-0, Sph-2.5, Sph-5, and Sph-10, respectively) did not significantly alter the apoptotic activity of MSCs (**Figure 3**a). Similarly, the expression of a proapoptotic gene, caspase-3, was not significantly changed by differences in

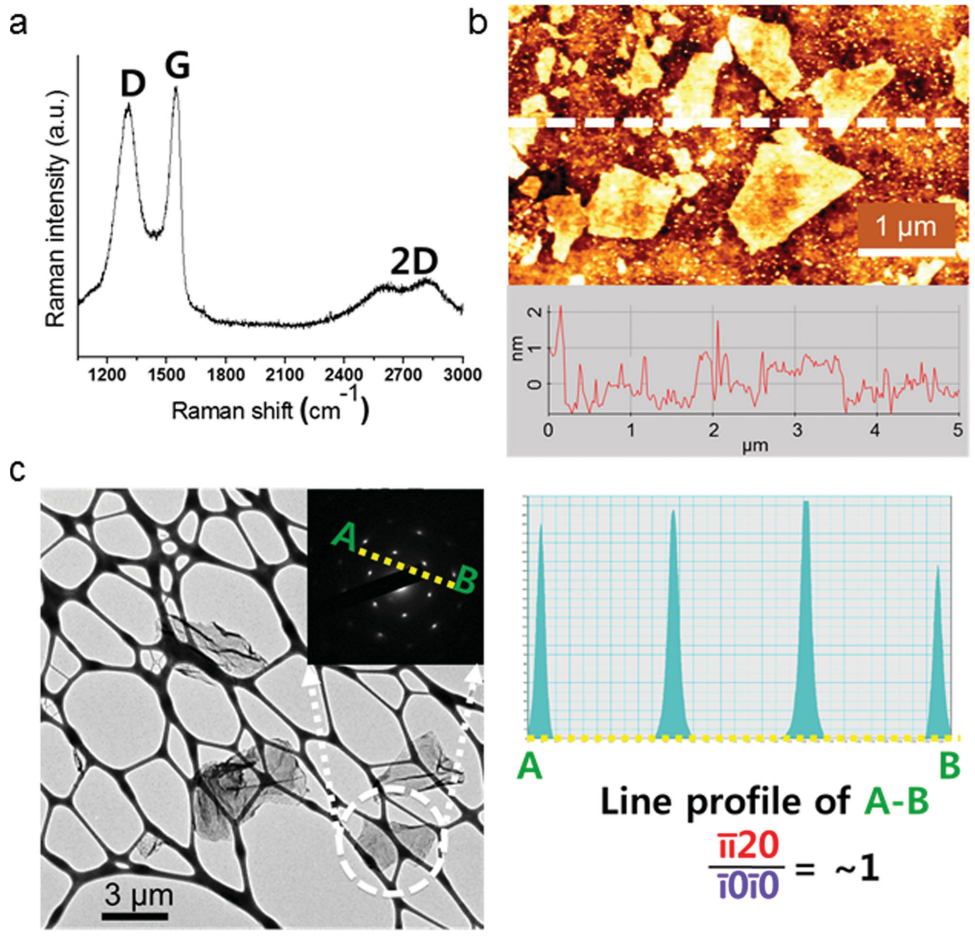

Figure 2. Characterization of RGO flakes. a) Raman spectroscopy, b) AFM image, and c) TEM image and corresponding SAED pattern of RGO flakes.

the RGO concentration (Figure 3b). However, the expression of the antiapoptotic gene Bcl-2 was decreased significantly in MSCs incorporated with 10 μg mL^{-1} RGO flakes (Figure 3b). A previous study has reported that increasing RGO concentration in cell culture can exert oxidative stress on the cells, and thus induce cell apoptosis.[24] We postulated that this could be the reason for the decreased Bcl-2 expression in MSCs incorporated with 10 μg mL^{-1} RGO flakes. Therefore, RGO concentrations lower than 10 μg mL^{-1} would be preferred for the formation of MSC–RGO hybrid spheroids. The cytotoxicity of incorporation

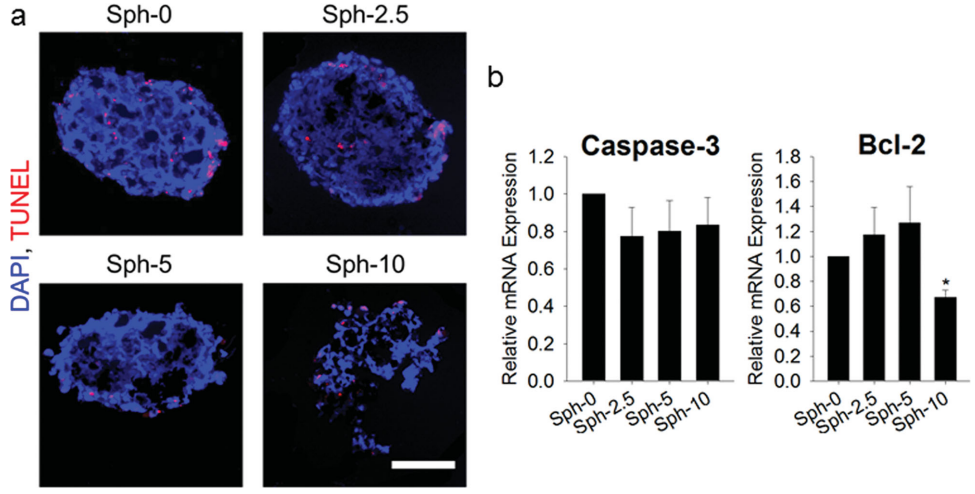

Figure 3. Cytotoxicity of RGO flakes. a) TUNEL staining of apoptotic cells in MSC spheroids that contain various amounts of RGO flakes. Scale bar, 100 μm. b) Relative mRNA expression of a proapoptotic gene, caspase-3, and an antiapoptotic gene, Bcl-2. *$p < 0.05$ versus any other group.

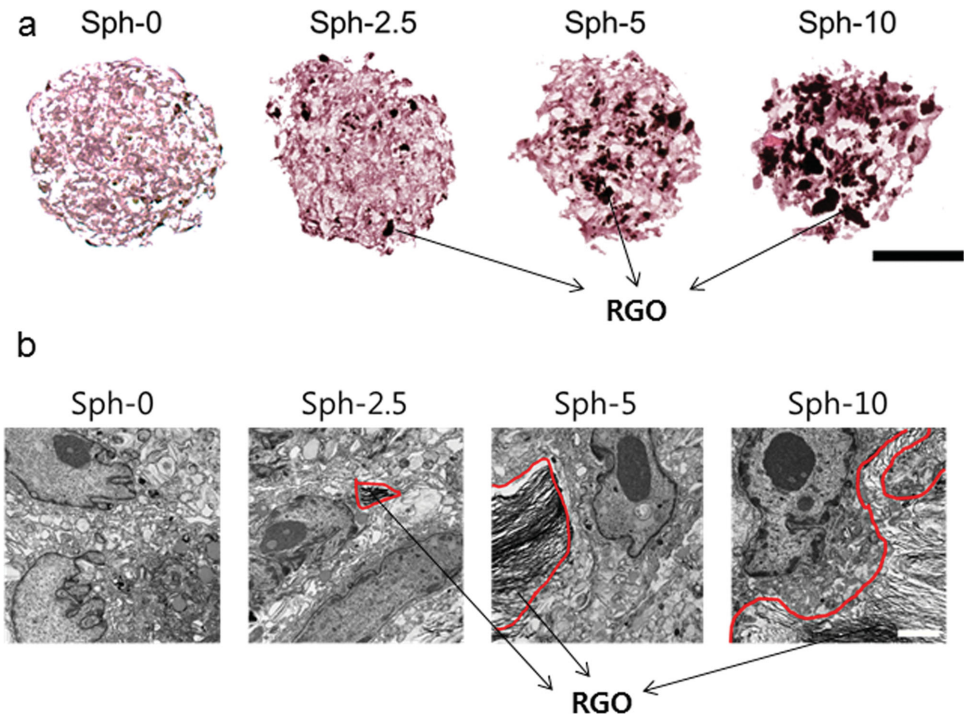

Figure 4. Formation of MSC–RGO hybrid spheroids that contain various amounts of RGO flakes. a) H&E staining of MSC–RGO hybrid spheroids. RGO flakes are indicated by black color. Scale bar, 100 μm. b) TEM images of MSC–RGO hybrid spheroids. Cell–RGO interactions were minimal in Sph-0 and Sph-2.5, and dominant in Sph-10. Sph-5 showed a good combination of cell–RGO and cell–cell interactions. Scale bar, 2 μm.

of 5 μg mL^{-1} RGO flakes was further analyzed by staining viable and nonviable cells using fluorescein diacetate (FDA) and ethidium bromide (EB), respectively. The FDA and EB staining demonstrated that the incorporation of 5 μg mL^{-1} RGO did not alter the viability of MSCs in spheroids (Figure S1a, Supporting Information). In addition, cell counting kit-8 (CCK-8) analyses of Sph-0 and Sph-5 showed that there was no significant difference in the cell viability in spheroids with and without 5 μg mL^{-1} RGO incorporation (Figure S1b, Supporting Information).

To examine the formation of MSC–RGO hybrid spheroids, hematoxylin and eosin (H&E) staining and TEM analysis were performed for Sph-0, Sph-2.5, Sph-5, and Sph-10. H&E staining of the spheroid sections showed that the distribution of RGO flakes within spheroids was quite homogenous (**Figure 4**a). The amount of RGO flakes incorporated in MSC spheroids increased with an increase in the RGO concentration in the MSC–RGO suspension in hanging drop form during the process of MSC–RGO hybrid spheroid formation (Figure 4a).

To examine the interaction of RGO flakes with MSCs in spheroids, TEM images were obtained (Figure 4b). In the absence of RGO flakes, the MSC spheroids (Sph-0) showed only cell–cell contacts. In contrast, cell–RGO contacts were dominant in Sph-10, and negligible cell–cell contacts were observed. In Sph-2.5 and Sph-5, cell–RGO and cell–cell contacts were observed. The comparison of these two types of hybrid spheroids revealed that Sph-5 showed a balanced combination of cell–cell and cell–RGO contacts, whereas Sph-2.5 showed mainly cell–cell contacts with very limited cell–RGO contacts. Therefore, considering the optimized combination of cell–cell and cell–RGO contacts along with the cytotoxicity data, an RGO concentration of 5 μg mL^{-1} was chosen for the formation of MSC–RGO hybrid spheroids in the following experiments.

2.3. Enhanced Cell–ECM Interaction by RGO Incorporation into MSC Spheroids

A previous study has demonstrated that cell adhesion to graphene substrates is mediated by cell–ECM interactions due to the adsorption of ECM proteins, such as FN, to graphene.[25] Therefore, we evaluated the capability of RGO flakes to adsorb FN from a serum-containing culture medium. While no FN was detected in RGO flakes immersed in phosphate buffered saline (PBS), a significant amount of FN was detected in RGO flakes incubated in serum-containing culture medium (**Figure 5**a). The expression of FN was detectable only at the periphery of MSC spheroids without RGO (Figure 5b), which is in agreement with the results of a previous study.[26] In contrast, FN was distributed evenly throughout the MSC–RGO hybrid spheroids in Sph-5 (Figure 5b), because the RGO flakes in the hybrid spheroids adsorbed FN. FN in the MSC–RGO hybrid spheroids (Sph-5) can provide cell–ECM interactions via FN-integrin binding,[27] To confirm the enhanced cell–ECM interactions obtained through the incorporation of FN-adsorbed RGO flakes into MSC spheroids, we examined the expression of integrin β1, an integrin type that is known to bind to FN for cell–FN interactions.[28] As expected, integrin β1 was significantly enhanced in Sph-5 compared with Sph-0 (Figure 5c).

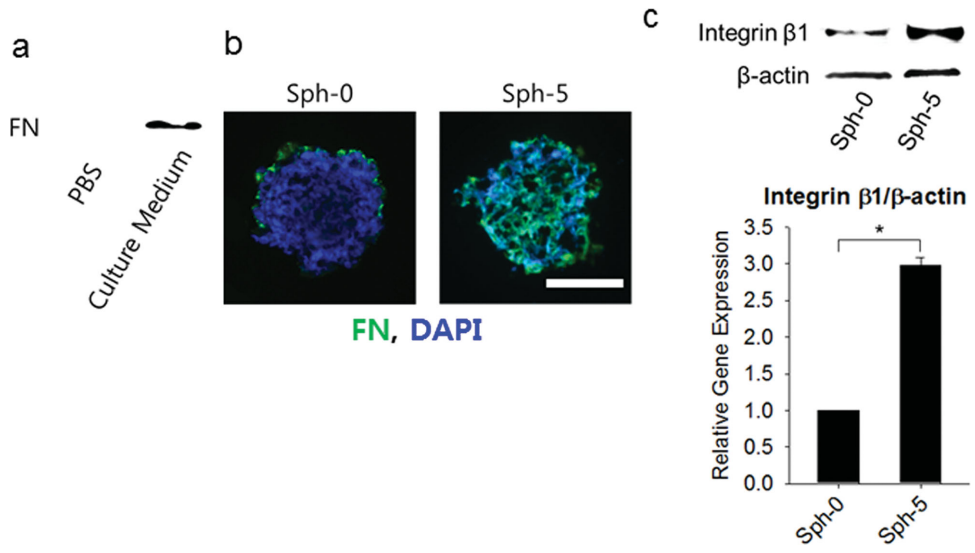

Figure 5. Incorporation of RGO flakes into MSC spheroids provides cell–ECM interactions. a) Incubation of RGO flakes in a serum-containing culture medium resulted in FN adsorption on the RGO flakes, whereas incubation in PBS resulted in no adsorption, as determined by western blot analysis. b) A homogenous distribution of FN was observed in the MSC–RGO hybrid spheroids, which can provide cell–ECM interactions, whereas FN was detected only at the periphery of MSC spheroids, as determined by immunohistochemistry for FN. Scale bar, 100 μm. c) Enhanced expression of integrin $\beta 1$, a FN-interacting integrin, was observed in MSC–RGO hybrid spheroids, indicating enhanced cell–FN interaction, as determined by western blot analysis. $^{*}p < 0.05$.

2.4. Enhanced Angiogenic Growth Factor Expression in MSC–RGO Spheroids

Enhanced cell–ECM interactions trigger cell signaling cascades that upregulate the expression of growth factors.[18] Integrin-mediated cell–ECM interactions facilitate focal adhesion kinase (FAK) activation.[29] The phosphorylation of FAK (pFAK) activates extracellular signal-regulated kinase (ERK) thereby enhances VEGF expression.[30] In this study, the incorporation of RGO flakes into MSC spheroids enhanced the cell–ECM interaction mediated by FN-integrin binding (Figure 5c), which led to enhanced expressions of pFAK, phosphorylated ERK (pERK), and thus, VEGF (**Figure 6**a).

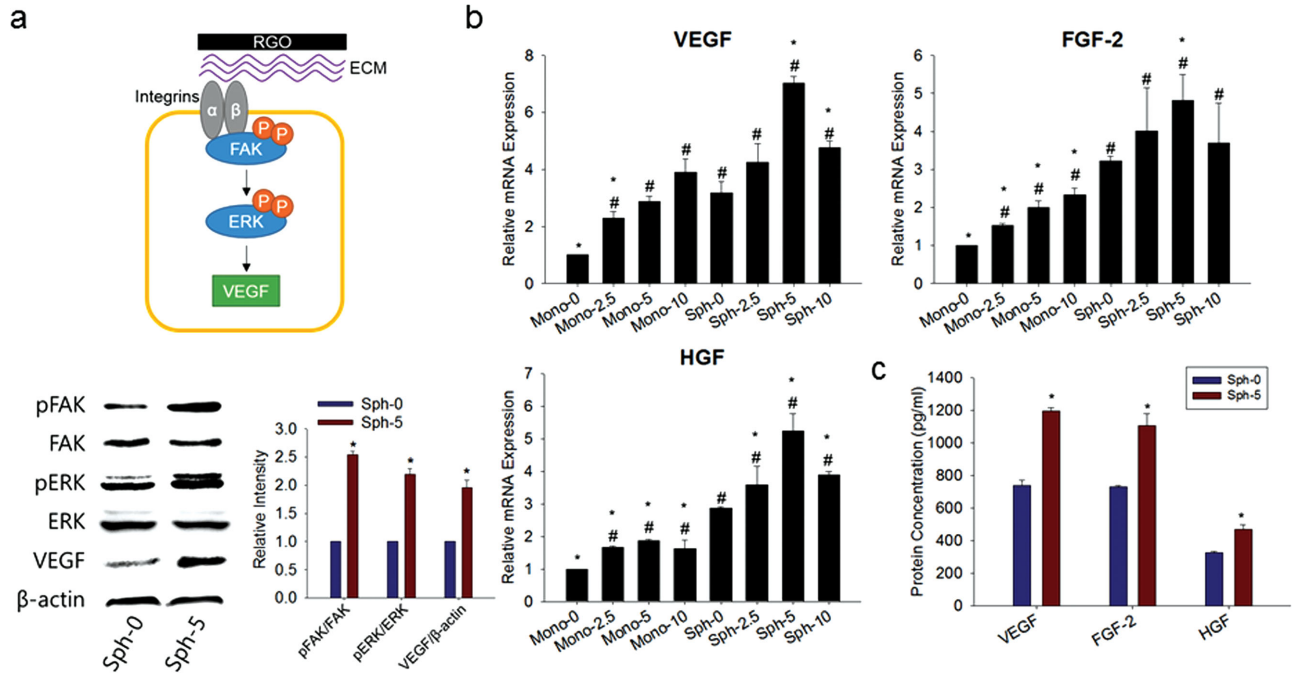

Figure 6. Enhanced angiogenic factor expression in MSC–RGO hybrid spheroids. a) Changes in the expression of cell signaling molecules due to RGO incorporation. b) mRNA expression of angiogenic growth factors evaluated by qRT–PCR. c) Amounts of secreted growth factors determined by ELISA. $^{\#}p < 0.05$ versus Mono-0 (monolayer culture that contains 0 μg mL^{-1} RGO flakes.) $^{*}p < 0.05$ versus Sph-0.

We examined the expression of angiogenic growth factors through quantitative reverse transcription polymerase chain reaction (qRT–PCR) and enzyme-linked immunosorbent assay (ELISA). VEGF, FGF-2, and hepatocyte growth factor (HGF) were analyzed because these are the major growth factors that induce angiogenesis,[31] which plays a critical role in cardiac repair.[32] The expression of VEGF, FGF-2, and HGF showed similar tendencies (Figure 6b). The formation of spheroids enhanced the expression of proangiogenic growth factors compared with that obtained with a monolayer culture (Sph-0 versus Mono-0, Figure 6b), which is in accordance with previously reported results.[33] This finding is attributed to the activation of E-cadherin in the MSC spheroids by enhanced cell–cell interactions.[10] More importantly, we demonstrate for the first time that the addition of RGO flakes to cell culture further enhances the expression of the growth factors, in both monolayer and spheroid cultures (Figure 6b). As a result, spheroid formation and RGO incorporation additively enhanced the expression of growth factors (Figure 6b). The expression of growth factors was highest in the hybrid spheroids with 5 μg mL^{-1} RGO flakes (Figure 6b). This result is likely because cell–cell and cell–ECM interactions, which upregulate the expression of growth factors, in MSC spheroids are optimal and that RGO is not cytotoxic at an RGO concentration of 5 μg mL^{-1} (Figure 3, 4). Similar to the gene expression data, MSC–RGO hybrid spheroids with 5 μg mL^{-1} RGO flakes (Sph-5) showed significantly enhanced secretion of paracrine factors compared with spheroids without RGO (Figure 6c). To the best of our knowledge, this study provides the first demonstration that RGO enhances the secretion of growth factors.

Hypoxia is known to stimulate the growth factor expression of the cells in spheroids.[33] Hypoxia, which is caused by the limited diffusion of oxygen,[34] is dependent on the size of the spheroids. In this study, the quantification of the spheroid sizes showed that the sizes were not influenced by the incorporation of RGO flakes (Figure S2, Supporting Information). Therefore, the effect of hypoxia on MSC functions induced by RGO incorporation was not investigated in this study.

2.5. Enhanced Cx43 Expression in MSC–RGO Spheroids

MI not only causes fibrosis of the heart but also may trigger ventricular arrhythmia due to electrical remodeling of the heart.[35] Excessive deposition of fibrotic tissue and loss of functional cardiac cells impair linear electrical propagation and lead to arrhythmia,[36] at least in part, due to a reduced level of Cx43.[37] Therefore, postinjury arrhythmia may be reduced by activating Cx43.[38] In addition, the engraftment of Cx43-expressing cells into the infarct region can reduce the propensity for arrhythmogenesis.[4] However, the expression of Cx43 in naïve MSCs is very low,[5] possibly limiting the antiarrhythmogenic potential of MSC therapy. In addition, Hahn et al. showed that MSCs with augmented Cx43 expression exert an enhanced cytoprotective effect on cardiomyocytes, reduce the infarct size, and improve cardiac function.[7]

It has been previously reported that VEGF[19] and electrically conductive materials[39] can enhance the expression of Cx43. In the present study, RGO incorporation into MSC spheroids increased VEGF expression (Figure 6). In addition, RGO is an electrically conductive material.[40] Therefore, we hypothesized that MSC–RGO hybrid spheroids upregulate Cx43 expression compared with MSC spheroids without RGO, likely due to increased VEGF expression and the conductivity of RGO flakes (**Figure 7**a).

To test this hypothesis, Cx43 expression was assessed in MSC spheroids with or without RGO. The qRT–PCR analysis indicated that Sph-5 and Sph-10 showed the highest Cx43 mRNA expression levels (Figure 7b). The western blot analysis showed that the protein level of Cx43 was also enhanced by RGO incorporation (Figure 7c). The immunostaining of Cx43 demonstrated that Cx43 was hardly observed in Sph-0 and Sph-2.5 (Figure 7d). In contrast, Cx43 was found to be well expressed in Sph-5 and Sph-10 (Figure 7d). To verify that the conductivity of RGO contributes to the upregulation of Cx43, we compared the Cx43 expression levels between RGO-incorporated spheroids (Sph–RGO) and GO-incorporated spheroids (Sph–GO). GO is electrically insulating and RGO is conductive.[41] For this comparison, we used GO flakes with dimensions that are similar to those of the RGO flakes. Despite the abilities of GO to adsorb FN and activate FAK,[25] which resemble those of RGO (Figures 5a and 6a), GO significantly reduced the Cx43 expression in MSCs (Figure 7e). This finding demonstrates that the conductivity of RGO indeed contributes to the upregulation of Cx43. The functionality of Cx43 was examined by dye transfer analysis. We labeled half of the MSCs with DiI and the other half of the MSCs with calcein acetoxymethyl ester (AM), which is transferred to adjacent cells through Cx43,[42] and then used these cells to form spheroids. If functional gap junctions exist, calcein AM would transfer to adjacent cells.[43] In Sph-0, no notable dye transfer was observed (Figure 7f). In contrast, the transfer of calcein AM to DiI-labeled MSCs was observed in Sph-5 (Figure 7f). These results demonstrate that the presence of functional gap junctions in Sph-5.

Although other conductive materials that can adsorb proteins could also promote paracrine factor secretion and Cx43 expression, it is hard to process the materials into thin, 2D shape. For example, gold is generally fabricated into nano-[44] or microsized particles.[45] However, gold nanoparticles would not be able to provide cell–ECM interactions because the nanoparticles would be easily uptaken by the cells.[46] On the other hand, the use of microparticles would require a larger amount of conductive materials to provide cell–ECM interactions compared with the use of 2D flakes due to the lower ratio of surface area to volume, which would not be appropriate for in vivo implantation.

2.6. Improved Cardiac Repair by MSC–RGO Hybrid Spheroid Implantation

In general, the number of MSCs implanted to mouse MI model ranges between 5×10^5 and 5×10^6 cells.[47] Meanwhile, in the present study, we implanted 3×10^5 MSCs per mouse. This dose of MSCs was implanted to demonstrate that the incorporation of RGO flakes was able to show a significant therapeutic efficacy even with the reduced amount of the implanted cells.

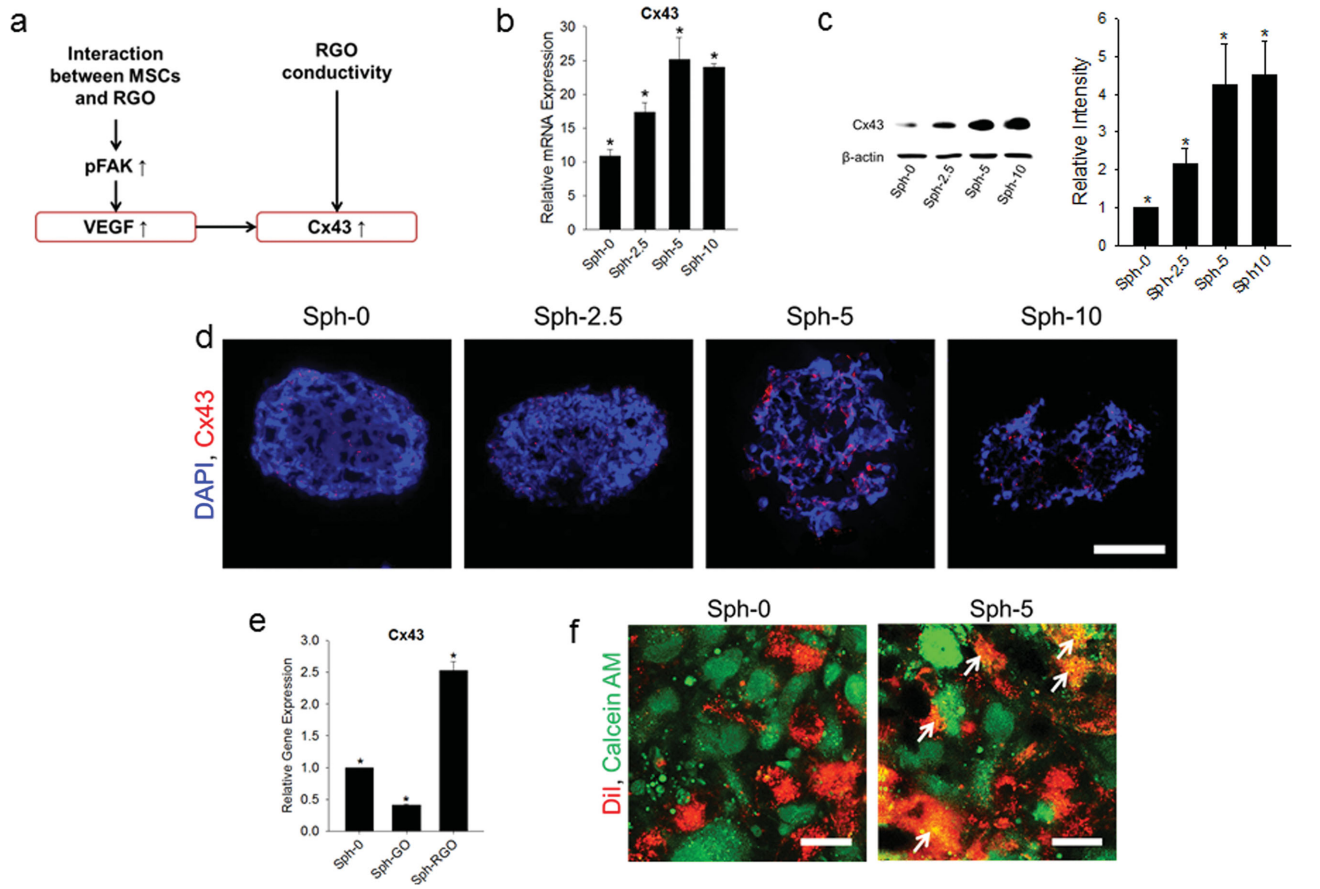

Figure 7. Enhanced Cx43 expression in MSC–RGO hybrid spheroids. a) Schematic diagram of mechanisms for enhanced Cx43 expression through RGO incorporation into MSC spheroids.[19,39] b) qRT–PCR analyses of Cx43 expression. c) Cx43 protein expression analyzed by western blot. d) Immunostaining of Cx43 in MSC spheroids incorporated with various concentrations of RGO flakes. Scale bar, 100 μm. e) Effect of incorporation of either nonconductive GO flakes or conductive RGO flakes into MSC spheroids on Cx43 expression in the MSCs, as evaluated by qRT–PCR analyses. f) Dye transfer analysis of Sph-0 and Sph-5. The arrows (yellow) show the transfer of calcein AM (green) dye from calcein AM-labeled MSCs to DiI (red)-labeled MSCs. Calcein AM is known to transfer to neighboring cells through functional gap junctions (Cx43).[42] Scale bars, 20 μm. $*p < 0.05$ versus any other group.

The amount of RGO flakes implanted to a mouse is ≈0.75 mg RGO kg^{-1} mouse body weight. This RGO amount is much lower than 20 mg kg^{-1} which has been reported to exhibit no appreciable in vivo toxicity.[48] In addition, our in vitro data demonstrated that there was no significant induction of cell apoptosis or reduction in cell functions such as secretion of paracrine factors (Figures 3 and 6). Therefore, although RGO flakes are not biodegradable,[49] the amount of RGO flakes used for in vivo implantation in this study would not exhibit significant toxicity.

Vascularization was evaluated by determining the density of capillaries in the border zone of infarcted myocardium 14 d after cell implantation. Capillaries were identified by immunohistochemical staining with antibodies specific to von Willebrand factor (vWF). Although the MSC spheroids (Sph-0) were able to promote angiogenesis compared with the injection of either PBS or RGO flakes, the MSC–RGO hybrid spheroids (Sph-5) further enhanced the vascularization in the infarcted myocardium (**Figure 8**a). This result may be attributed to the enhanced secretion of angiogenic growth factors in MSCs obtained by the incorporation of RGO flakes (Figure 6b,c).

The promotion of angiogenesis attenuates cardiac remodeling after MI.[32] In this study, the incorporation of RGO flakes into MSC spheroids enhanced vascularization and attenuated cardiac remodeling. Masson's trichrome staining of the longitudinal sections of the heart was performed 14 d after the treatment to quantify the fibrous tissue area (Figure 8b). The results showed large fibrotic areas (blue) in the PBS and RGO groups and a small fibrotic area in the Sph-0 group. Importantly, the implantation of Sph-5 showed the smallest fibrotic area, which indicates attenuated cardiac remodeling.

To evaluate the electrical remodeling of the heart, the expression of Cx43 in the border zone of the infarcted myocardium was analyzed. Cx43 is the most abundant type of connexin and is a critical determinant for the electrical properties of the heart.[50] It has been reported that the enhanced expression of Cx43 in implanted cells contributes to the prevention of postinfarct arrhythmia.[4] In the PBS and RGO groups, the expression levels of Cx43 were relatively low (Figure 8c). Although Sph-0 showed an increase in Cx43 expression, a marked increase in the Cx43 level was apparent in the Sph-5 group. Therefore, the incorporation of RGO flakes into MSC

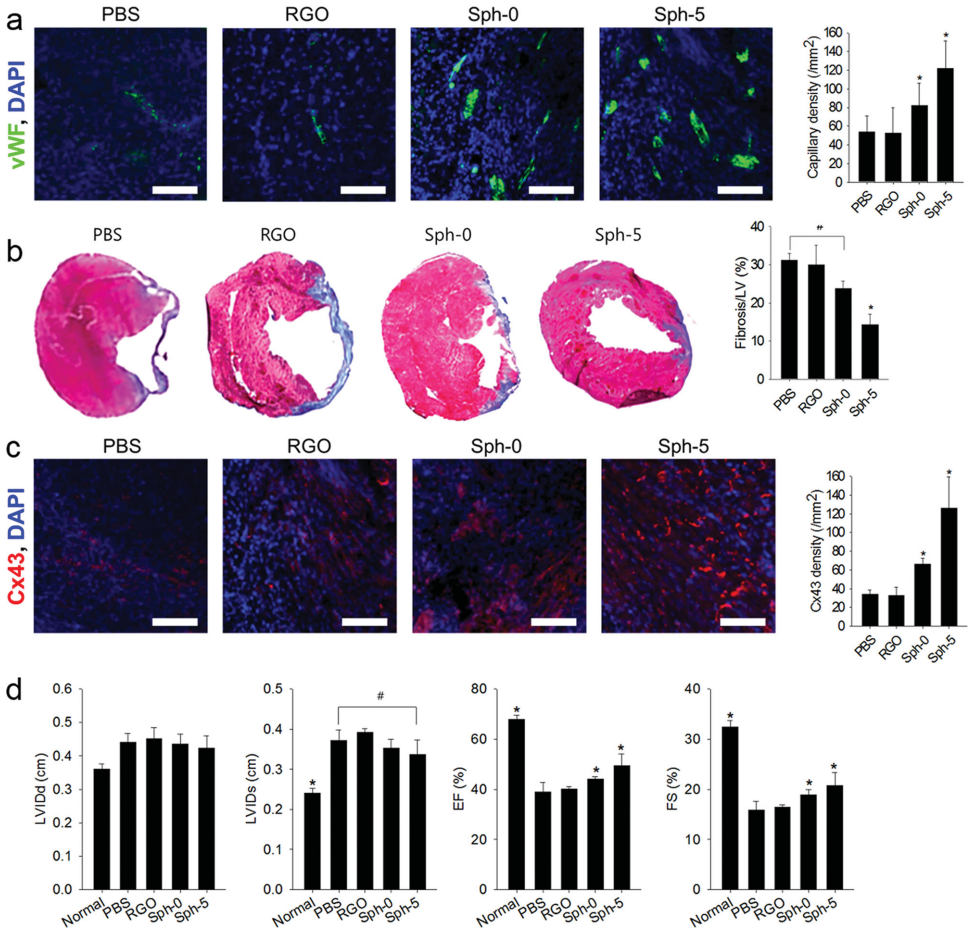

Figure 8. Enhanced cardiac repair and cardiac function restoration by implantation of MSC–RGO hybrid spheroids. Infarcted hearts were treated through the injection of PBS, RGO flakes, MSC spheroids (Sph-0), or MSC–RGO hybrid spheroids (Sph-5). a) Capillary density in the periinfarct border zone assessed by immunostaining for vWF (green). Scale bars, 100 μm. b) Cardiac fibrosis indicated by Masson's trichrome staining (blue) and quantification of the fibrotic area. c) Expression of Cx43 (red) examined by immunohistochemical staining in the infarct border zone. Scale bars, 100 μm. d) Cardiac functions analyzed by echocardiography. $^{*}p < 0.05$ versus any other group. $^{\#}p < 0.05$.

spheroids attenuated the electrical remodeling of the heart after MI.

2.7. Improvement in Cardiac Function by MSC–RGO Hybrid Spheroid Implantation

The implantation of Sph-5 improved cardiac function, as demonstrated through transthoracic echocardiography of the infarcted hearts 14 d after the treatment. (Figure 8d). In terms of ejection fraction (EF) and fractional shortening (FS), RGO itself did not exert any therapeutic effect. There was no significant difference in the left ventricular internal diameter at end diastole (LVIDd) between the groups. Although the implantation of Sph-0 and Sph-5 showed significantly improved EF and FS, along with the reduction of fibrosis, remarkable improvement in cardiac functions was observed in the Sph-5 group compared with the Sph-0 group. The EF was higher in the Sph-5 group (49.6% ± 4.6%, $p < 0.05$) compared with the Sph-0 group (44.2% ± 0.9%, $p < 0.05$) and the PBS group (38.9% ± 3.7%, $p < 0.05$). The adverse cardiac remodeling was also attenuated in the Sph-5 group, showing a significant reduction of left ventricular internal diameter at end systole (LVIDs) compared with the PBS group (Figure 8d). Collectively, echocardiographic parameters showed better cardiac performance in the Sph-5 group than in the Sph-0 group.

3. Conclusions

The incorporation of RGO flakes into MSC spheroids promoted the expression of angiogenic growth factors and Cx43 in the MSCs, both of which are important for cardiac repair, likely due to their high affinity toward FN and the high electrical conductivity of RGO. The implantation of MSC–RGO hybrid spheroids into the infarcted myocardium enhanced cardiac repair and cardiac function restoration compared with the injection of either RGO flakes or MSC spheroids. Therefore, RGO can enhance the therapeutic efficacy of MSCs for the treatment of MI.

4. Experimental Section

RGO Preparation and Analyses: Graphite powder (<20 μm) was purchased from Sigma-Aldrich and used as received. GO was synthesized using a modified Hummers method.[51] The synthesized GO was suspended in water (0.05 wt%) to give a brown dispersion. The exfoliation of GO was achieved by ultrasonication for 3 h, and the mixture was subsequently dialyzed (12–14 kDa cut-off) for 6 h to remove any residual salts and acids. The obtained solution was then subjected to centrifugation at 3000 rpm for 20 min to remove the unexfoliated GO. The resulting homogeneous dispersion (100 mL) was mixed with 1 mL of hydrazine solution (35 wt% in water) and 7 mL of ammonia solution (28 wt% in water). RGO powder was then obtained by filtration and drying in vacuum. The RGO samples were characterized by Raman spectroscopy, AFM, TEM, and SAED. The Raman spectra were recorded using an argon ion laser (514 nm) as the excitation source with a notch filter of 50 cm^{-1}. The typical scan ranged from 1000 to 3000 cm^{-1} and the instrumental resolution was 10 cm^{-1}. The surface morphology of the RGO samples was examined using the noncontact mode AFM (XE-100 system, Park Systems, Korea). TEM and SAED were conducted with a TEM (JEOL 2100, JEOL, Japan) operated at 200 kV installed at the National Center for Inter-university Research Facilities at Seoul National University. The rotation between the TEM images and the corresponding SAED patterns was calibrated using molybdenum trioxide crystals.

MSC–RGO Spheroid Formation: Human bone marrow-derived MSCs were purchased from a commercial source (Lonza, USA) and cultured in Dulbecco's modified Engle's Medium (DMEM, Gibco BRL, USA) containing 10% (v/v) fetal bovine serum (FBS; Gibco-BRL) and 1% (v/v) penicillin–streptomycin (PS; Gibco-BRL) on cell culture plates. MSC or MSC–RGO spheroids were fabricated through the hanging-drop method with slight modifications.[52] Three thousand MSCs (passage 5) in 30 μL of DMEM containing 20% (v/v) FBS, 1% (v/v) PS, and RGO (0, 2.5, 5, or 10 μg mL^{-1}) were incubated hanging on the lid of a Petri dish for two days to form a spheroid. To evaluate the morphology of the spheroids and the presence of RGO in the spheroids, the spheroids were fixed in 4% (v/v) paraformaldehyde for 30 min and embedded in optimal cutting temperature (OCT) compound. The spheroids were cut into 10-μm sections and stained with H&E. Cell apoptosis was evaluated using a TUNEL assay kit (Millipore Corp., Billerica, MA, USA) according to the manufacturer's instructions. For comparison, MSCs were cultured on a cell culture plate in a monolayer, and incubated with RGO flakes (0, 2.5, 5, or 10 μg mL^{-1}) for two days (Mono-0, Mono-2.5, Mono-5, and Mono-10, respectively).

TEM Analyses: The spheroids were fixed with Karnovsky's solution (EMS Hatfield, PA, USA) for 24 h at 4 °C and washed three times with a 0.05 M sodium cacodylate buffer. The specimens were then fixed with 2% osmium tetroxide (Sigma) for 2 h at 4 °C, washed three times with cold distilled water, dehydrated through a series of graded ethanol (50%, 60%, 70%, 80%, 90%, 95%, 98%, and 100%) and propylene oxide rinses, and finally embedded in Spurr's resin (Agar Scientific, Essex, UK). The samples were then polymerized at 60 °C for 24 h and cut into thin slices using an ultramicrotome (MTX, RMC, Arizona, USA). The thin sections were observed with a Libra 120 microscope (Carl Zeiss, Oberkochen, Germany).

qRT–PCR: The total RNA was extracted using 1 mL of TRIzol reagent (Invitrogen) and 200 μL of chloroform. The samples were centrifuged at 12 000 rpm at 4 °C for 10 min. The RNA pellets were washed with 75% (v/v) ethanol and dried. After the drying procedure, the samples were dissolved in RNase-free water. The RNA (500 ng) from each sample was reverse-transcribed to obtain cDNA using GoScript Reverse Transcriptase (Promega, USA). SYBR green-based qRT–PCR was performed using a StepOnePlus Real-Time PCR System (Applied Biosystems, USA) instrument with the TOPreal qPCR Premix (Enzynomics, Korea). Forty amplification cycles were performed, and each cycle consisted of three steps: 30 s at 94 °C, 45 s at 55 °C, and 45 s at 72 °C. The primer sequences for the qRT–PCR analyses are listed in **Table 1**. All of the data were analyzed using the $2^{-\Delta\Delta Ct}$ method. Three samples were analyzed per group.

Table 1. Primer sequences.

Gene	Forward primer	Reverse primer
Glyceraldehyde 3-phosphate dehydrogenase	5′-CCA CTC CTC CAC CTT TGA C-3′	5′-ACC CTG TTG CTG TAG CCA-3′
Bcl-2	5′-TTG GCC CCC GTT GCT T-3′	5′-CGG TTA TCG TAC CCT GTT CTC-3′
Caspase-3	5′-GGT TTT CGG TGG GTG T-3′	5′-CAG TGT TCT CCA TGG ATA CCT-3′
VEGF	5′-GAG GGC AGA ATC ATC ACG-3′	5′-CAC CAG GGT CTC GAT TGG AT-3′
FGF-2	5′-GAC GGC CGA GTT GAC GG-3′	5′-CTC TCT CTT CTG CTT GAA GTT-3′
HGF	5′-GAT GGC CAG CCG AGG C-3′	5′-TCA GCG CAT GTT TTA ATT GCA-3′
Cx43	5′-TCT GAG TGC CTG AAC TTG C-3′	5′-ACT GAC AGC CAC ACC TTC C-3′

Analyses of Cell Viability: FDA and EB solution was prepared by mixing 10 μL FDA solution (Sigma, 5 mg mL^{-1} in acetone) and 10 mL EB solution (Sigma, 10 μg mL^{-1} in PBS). Sph-0 and Sph-5 were incubated in FDA and EB solution for 3–5 min at 37 °C. After staining, the samples were examined using a fluorescence microscope (IX71 inverted microscope, Olympus, Tokyo, Japan). The cell viability was quantitatively measured using CCK-8 (Sigma).

ELISA: The spheroids were incubated in DMEM without FBS for 24 h. The amount of growth factors in the supernatant was then determined quantitatively using an ELISA assay kit ($n = 3$ per group, R&D Systems, USA).

Western Blot: The analysis was performed through 10% (w/v) sodium dodecyl sulfate–polyacrylamide gel electrophoresis ($n = 3$ per group). The proteins were first transferred to an Immobilon-P membrane (Millipore Corp., USA) and then probed with antibodies against pFAK, VEGF, CX43, and β-actin (all purchased at Abcam, UK). The proteins were then incubated with a horseradish peroxidase-conjugated secondary antibody (Santa Cruz Biotechnology, USA) for 1 h at room temperature. The blots were developed using an enhanced chemiluminescence detection system (Amersham Bioscience, USA).

Immunocytochemistry: The spheroid sections were immunocytochemically stained with antibodies against Cx43 (Abcam). The immunostaining signal was visualized with rhodamine isothiocyanate-conjugated secondary antibodies (Jackson ImmunoResearch Laboratories, USA). The slides were counterstained with DAPI (Vector Laboratories, USA) to stain the nuclei of the cells.

Dye Transfer: MSCs were stained with either 10×10^{-6} M DiI or 10×10^{-6} M Calcein AM. After washing, the DiI-labeled MSCs and Calcein AM-labeled MSCs with or without RGO (5 μg mL^{-1}) were mixed in equal proportions to form spheroids. The spheroids were imaged using a Leica TCS SP8 X Confocal Microscope (Leica Microsystems, Mannheim, Germany).

MI Induction and Cell Implantation: The animal experimental protocol was approved by the Chonnam National University Animal Care and Use Committee (CNU IACUC-H-2014-22). MI was induced in 8-week-old male athymic BALB/c nude (nu/nu) mice ($n = 8$ per group, Central Lab Animal Inc., Seoul, Korea) by occlusion of the coronary artery. Briefly, the mice were anesthetized with an intramuscular injection of ketamine (50 mg kg^{-1}) and xylazine (10 mg kg^{-1}), and the left coronary artery was occluded within the myocardium between the left atrial appendage and the right ventricular outflow tract using a curved needle and a 5-0 silk suture. One week after MI, PBS, RGO flakes, Sph-0 (3×10^5 cells), or Sph-5 (3×10^5 cells) in a volume of 50 μL were injected into the border zone. Age-matched mice that were subjected to a sham operation were used as the non-MI group. The mice were sacrificed two days after MSC implantation.

Histochemical and Immunohistochemical Staining: Two weeks after cell injection, the hearts were excised and transversely sectioned into two blocks across the infarct zone. The tissue blocks were frozen in liquid nitrogen with the Tissue-Tek OCT compound, and sectioned to 4-μm-thick sections. For immunohistochemical analysis, the slides were treated with 3% hydrogen peroxide in PBS for 10 min at room temperature to block endogenous peroxidase activity. After nonspecific binding was blocked with 5% normal goat serum (Sigma), the slides were incubated with primary antibodies against Cx43 (Abcam, Cambridge, MA, USA) or vWF (Abcam) for 18 h at 4 °C. The sections were washed three times with PBS and then incubated for 1 h with Alexa-Fluor 488- or 594-conjugated-secondary antibodies. After washing, the slides were mounted with a mounting medium (VectaMount mounting medium, Vector Labs Inc., Burlingame, CA, USA). Images were obtained and digitized on a computer using an Olympus CX31 microscope (Olympus) equipped with an Infinity 1 camera (Lumenera Scientific, Ottawa, Canada). Five mice were analyzed for quantification. Cardiac fibrosis was evaluated by Masson's Trichrome staining. The fibrotic areas were determined by visualizing the blue-stained fibrotic deposits using the NIS-Elements Advanced Research program (Nikon, Japan). The percentage of ventricular fibrosis was calculated as the blue-stained area divided by the total ventricular area. Three samples were analyzed per group.

Evaluation of Cardiac Function: Left ventricular function was assessed by transthoracic echocardiography (n = 5 per group). Two weeks after spheroid injection, the animals were anesthetized and intubated. Echocardiography was performed to evaluate the left ventricular function. The echocardiography was performed with a 15-MHz linear array transducer system (iE33 system, Philips Medical Systems) by an expert who was not aware of the experimental conditions to exclude bias.

Statistical Analysis: The quantitative data are expressed as the means ± standard deviations. The statistical analyses were performed through one-way analysis of variance with Tukey's significant difference post hoc test using the SPSS software (SPSS Inc., USA). A value of $p < 0.05$ was considered to denote statistical significance.

Supporting Information

Supporting Information is available from the Wiley Online Library or from the author.

Acknowledgements

J.P. and Y.S.K. contributed equally to this work. This study was supported by a grant (2014029716) from the National Research Foundation of Korea and grants (HI12C0199 and HI14C1550) from the Korea Health 21 R&D Project, Ministry of Health and Welfare, Republic of Korea.

Received: January 28, 2015
Revised: February 23, 2015
Published online: March 19, 2015

[1] D. Orlic, J. Kajstura, S. Chimenti, I. Jakoniuk, S. M. Anderson, B. Li, J. Pickel, R. McKay, B. Nadal-Ginard, D. M. Bodine, A. Leri, P. Anversa, *Nature* **2001**, *410*, 701.

[2] a) B. Zhou, L. B. Honor, H. M. He, Q. Ma, J. H. Oh, C. Butterfield, R. Z. Lin, J. M. Melero-Martin, E. Dolmatova, H. S. Duffy, A. von Gise, P. Z. Zhou, Y. W. Hu, G. Wang, B. Zhang, L. C. Wang, J. L. Hall, M. A. Moses, F. X. McGowan, W. T. Pu, *J. Clin. Invest.* **2011**, *121*, 1894; b) N. Nagaya, K. Kangawa, T. Itoh, T. Iwase, S. Murakami, Y. Miyahara, T. Fujii, M. Uematsu, H. Ohgushi, M. Yamagishi, T. Tokudome, H. Mori, K. Miyatake, S. Kitamura, *Circulation* **2005**, *112*, 1128; c) T. Kinnaird, E. Stabile, M. S. Burnett, C. W. Lee, S. Barr, S. Fuchs, S. E. Epstein, *Circ. Res.* **2004**, *94*, 678; d) M. Gnecchi, H. He, N. Noiseux, O. D. Liang, L. Zhang, F. Morello, H. Mu, L. G. Melo, R. E. Pratt, J. S. Ingwall, V. J. Dzau, *FASEB J.* **2006**, *20*, 661; e) C. Gandia, A. Arminan, J. M. Garcia-Verdugo, E. Lledo, A. Ruiz, M. D. Minana, J. Sanchez-Torrijos, R. Paya, V. Mirabet, F. Carbonell-Uberos, M. Llop, J. A. Montero, P. Sepulveda, *Stem Cells* **2008**, *26*, 638.

[3] S. de Jong, T. A. van Veen, H. V. van Rijen, J. M. de Bakker, *J. Cardiovasc. Pharmacol.* **2011**, *57*, 630.

[4] W. Roell, T. Lewalter, P. Sasse, Y. N. Tallini, B. R. Choi, M. Breitbach, R. Doran, U. M. Becher, S. M. Hwang, T. Bostani, J. von Maltzahn, A. Hofmann, S. Reining, B. Eiberger, B. Gabris, A. Pfeifer, A. Welz, K. Willecke, G. Salama, J. W. Schrickel, M. I. Kotlikoff, B. K. Fleischmann, *Nature* **2007**, *450*, 819.

[5] D. G. Wang, F. X. Zhang, W. Z. Shen, M. L. Chen, B. Yang, Y. Z. Zhang, K. J. Cao, *Int. J. Cardiol.* **2011**, *152*, 314.

[6] M. G. Chang, L. Tung, R. B. Sekar, C. Y. Chang, J. Cysyk, P. Dong, E. Marban, M. R. Abraham, *Circulation* **2006**, *113*, 1832.

[7] J. Y. Hahn, H. J. Cho, H. J. Kang, T. S. Kim, M. H. Kim, J. H. Chung, J. W. Bae, B. H. Oh, Y. B. Park, H. S. Kim, *J. Am. Coll. Cardiol.* **2008**, *51*, 933.

[8] I. A. Potapova, G. R. Gaudette, P. R. Brink, R. B. Robinson, M. R. Rosen, I. S. Cohen, S. V. Doronin, *Stem Cells* **2007**, *25*, 1761.

[9] S. H. Hsu, G. S. Huang, S. Y. F. Lin, F. Feng, T. T. Ho, Y. C. Liao, *Tissue Eng. Part A* **2012**, *18*, 67.

[10] E. J. Lee, S. J. Park, S. K. Kang, G. H. Kim, H. J. Kang, S. W. Lee, H. B. Leo, H. S. Kim, *Mol. Ther.* **2012**, *20*, 1424.

[11] a) B. W. Doble, E. Kardami, *Mol. Cell. Biochem.* **1995**, *143*, 81; b) M. Wang, J. Cai, F. Huang, M. Zhu, Q. Zhang, T. Yang, X. Zhang, H. Qian, W. Xu, *Int. J. Mol. Med.* **2015**, *35*, 367.

[12] H. H. Yoon, S. H. Bhang, T. Kim, T. Yu, T. Hyeon, B.-S. Kim, *Adv. Funct. Mater.* **2014**, *24*, 6455.

[13] K. Yamada, K. G. Green, A. M. Samarel, J. E. Saffitz, *Circ. Res.* **2005**, *97*, 346.

[14] a) K. S. Kim, Y. Zhao, H. Jang, S. Y. Lee, J. M. Kim, J. H. Ahn, P. Kim, J. Y. Choi, B. H. Hong, *Nature* **2009**, *457*, 706; b) C. Chung, Y. K. Kim, D. Shin, S. R. Ryoo, B. H. Hong, D. H. Min, *Acc. Chem. Res.* **2013**, *46*, 2211.

[15] M. Kharaziha, S. R. Shin, M. Nikkhah, S. N. Topkaya, N. Masoumi, N. Annabi, M. R. Dokmeci, A. Khademhosseini, *Biomaterials* **2014**, *35*, 7346.

[16] W. C. Lee, C. H. Y. X. Lim, H. Shi, L. A. L. Tang, Y. Wang, C. T. Lim, K. P. Loh, *ACS Nano* **2011**, *5*, 7334.

[17] W. C. Lee, C. H. Lim, H. Shi, L. A. Tang, Y. Wang, C. T. Lim, K. P. Loh, *ACS Nano* **2011**, *5*, 7334.

[18] E. A. Sheta, M. A. Harding, M. R. Conaway, D. Theodorescu, *J. Natl. Cancer Inst.* **2000**, *92*, 1065.

[19] R. C. Pimentel, K. A. Yamada, A. G. Kleber, J. E. Saffitz, *Circ. Res.* **2002**, *90*, 671.

[20] I. K. Moon, J. Lee, R. S. Ruoff, H. Lee, *Nat. Commun.* **2010**, *1*, 73.

[21] Q. Mu, G. Su, L. Li, B. O. Gilbertson, L. H. Yu, Q. Zhang, Y.-P. Sun, B. Yan, *ACS Appl. Mater. Interfaces* **2012**, *4*, 2259.

[22] S. Schrepfer, T. Deuse, H. Reichenspurner, M. P. Fischbein, R. C. Robbins, M. P. Pelletier, *Transplant. Proc.* **2007**, *39*, 573.

[23] S. S. Datta, D. R. Strachan, S. M. Khamis, A. T. C. Johnson, *Nano Lett.* **2008**, *8*, 1912.

[24] K. H. Liao, Y. S. Lin, C. W. Macosko, C. L. Haynes, *ACS Appl. Mater. Interfaces* **2011**, *3*, 2607.

[25] X. T. Shi, H. X. Chang, S. Chen, C. Lai, A. Khademhosseini, H. K. Wu, *Adv. Funct. Mater.* **2012**, *22*, 751.

[26] J. Seo, J. S. Lee, K. Lee, D. Kim, K. Yang, S. Shin, C. Mahata, H. B. Jung, W. Lee, S. W. Cho, T. Lee, *Adv. Mater.* **2014**.

[27] a) S. K. Hanks, M. B. Calalb, M. C. Harper, S. K. Patel, *Proc. Natl. Acad. Sci. U.S.A.* **1992**, *89*, 8487; b) A. J. Garcia, D. Boettiger, *Biomaterials* **1999**, *20*, 2427.
[28] F. J. Fogerty, S. K. Akiyama, K. M. Yamada, D. F. Mosher, *J. Cell Biol.* **1990**, *111*, 699.
[29] M. Toutant, A. Costa, J. M. Studler, G. Kadare, M. Carnaud, J. A. Girault, *Mol. Cell. Biol.* **2002**, *22*, 7731.
[30] S. K. Mitra, D. D. Schlaepfer, *Curr. Opin. Cell Biol.* **2006**, *18*, 516.
[31] S. H. Bhang, S. W. Cho, J. M. Lim, J. M. Kang, T. J. Lee, H. S. Yang, Y. S. Song, M. H. Park, H. S. Kim, K. J. Yoo, Y. Jang, R. Langer, D. G. Anderson, B. S. Kim, *Stem Cells* **2009**, *27*, 1976.
[32] N. Ma, C. Stamm, A. Kaminski, W. Li, H. D. Kleine, B. Muller-Hilke, L. Zhang, Y. Ladilov, D. Egger, G. Steinhoff, *Cardiovasc. Res.* **2005**, *66*, 45.
[33] S. H. Bhang, S. W. Cho, W. G. La, T. J. Lee, H. S. Yang, A. Y. Sun, S. H. Baek, J. W. Rhie, B. S. Kim, *Biomaterials* **2011**, *32*, 2734.
[34] C. C. Wang, C. H. Chen, S. M. Hwang, W. W. Lin, C. H. Huang, W. Y. Lee, Y. Chang, H. W. Sung, *Stem Cells* **2009**, *27*, 724.
[35] J. M. B. Pinto, P. A. Boyden, *Cardiovasc. Res.* **1999**, *42*, 284.
[36] R. Khan, R. Sheppard, *Immunology* **2006**, *118*, 10.
[37] a) S. Poelzing, D. S. Rosenbaum, *Am. J. Physiol. Heart Circ. Physiol.* **2004**, *287*, H1762; b) D. E. Gutstein, G. E. Morley, H. Tamaddon, D. Vaidya, M. D. Schneider, J. Chen, K. R. Chien, H. Stuhlmann, G. I. Fishman, *Circ. Res.* **2001**, *88*, 333.
[38] M. P. O'Quinn, J. A. Palatinus, B. S. Harris, K. W. Hewett, R. G. Gourdie, *Circ. Res.* **2011**, *108*, 704.
[39] J.-O. You, M. Rafat, G. J. C. Ye, D. T. Auguste, *Nano Lett.* **2011**, *11*, 3643.
[40] C. Gomez-Navarro, R. T. Weitz, A. M. Bittner, M. Scolari, A. Mews, M. Burghard, K. Kern, *Nano Lett.* **2007**, *7*, 3499.
[41] D. Vuluga, J. M. Thomassin, I. Molenberg, I. Huynen, B. Gilbert, C. Jerome, M. Alexandre, C. Detrembleur, *Chem. Commun.* **2011**, *47*, 2544.
[42] Y. S. Kim, Y. Ahn, J. S. Kwon, Y. K. Cho, M. H. Jeong, J. G. Cho, J. C. Park, J. C. Kang, *Cells Tissues Organs* **2012**, *195*, 428.
[43] J. Czyz, U. Irmer, G. Schulz, A. Mindermann, D. F. Hulser, *Exp. Cell Res.* **2000**, *255*, 40.
[44] M. Grzelczak, J. Perez-Juste, P. Mulvaney, L. M. Liz-Marzan, *Chem. Soc. Rev.* **2008**, *37*, 1783.
[45] Z. Li, V. Ravaine, S. Ravaine, P. Garrigue, A. Kuhn, *Adv. Funct. Mater.* **2007**, *17*, 618.
[46] B. D. Chithrani, A. A. Ghazani, W. C. Chan, *Nano Lett.* **2006**, *6*, 662.
[47] a) A. Behfar, S. Yamada, R. Crespo-Diaz, J. J. Nesbitt, L. A. Rowe, C. Perez-Terzic, V. Gaussin, C. Homsy, J. Bartunek, A. Terzic, *J. Am. Coll. Cardiol.* **2010**, *56*, 721; b) J. Jin, Y. Zhao, X. Tan, C. Guo, Z. Yang, D. Miao, *PLoS One* **2011**, *6*, e21005; c) N. Noiseux, M. Gnecchi, M. Lopez-Ilasaca, L. Zhang, S. D. Solomon, A. Deb, V. J. Dzau, R. E. Pratt, *Mol. Ther.* **2006**, *14*, 840.
[48] K. Yang, J. Wan, S. Zhang, Y. Zhang, S. T. Lee, Z. Liu, *ACS Nano* **2011**, *5*, 516.
[49] Y. Li, L. Feng, X. Shi, X. Wang, Y. Yang, K. Yang, T. Liu, G. Yang, Z. Liu, *Small* **2014**, *10*, 1544.
[50] a) S. P. Thomas, J. P. Kucera, L. Bircher-Lehmann, Y. Rudy, J. E. Saffitz, A. G. Kleber, *Circ. Res.* **2003**, *92*, 1209; b) J. Jalife, G. E. Morley, D. Vaidya, *J. Cardiovasc. Electrophysiol.* **1999**, *10*, 1649.
[51] W. S. Hummers, R. E. Offeman, *J. Am. Chem. Soc.* **1958**, *80*, 1339.
[52] D. Del Duca, T. Werbowetski, R. F. Del Maestro, *J. Neurooncol.* **2004**, *67*, 295.